

**Site-specific laser modification of MgO nanoclusters: Towards atomic-scale surface structuring**Kenneth M. Beck,<sup>1</sup> Matthias Henyk,<sup>1</sup> Chongmin Wang,<sup>1</sup> Paolo E. Trevisanutto,<sup>2</sup> Peter V. Sushko,<sup>2</sup> Wayne P. Hess,<sup>1</sup> and Alexander L. Shluger<sup>2</sup><sup>1</sup>*Pacific Northwest National Laboratory, P.O. Box 999, Richland, Washington 99352, USA*<sup>2</sup>*Department of Physics and Astronomy, University College London, London WC1E 6BT, United Kingdom*

(Received 16 May 2006; published 6 July 2006)

Direct neutral metal emission from MgO nanostructures is induced using laser light tuned to excite specific surface sites at energies well below the excitation threshold of the bulk material. We find that near UV excitation of MgO nanocrystalline films and nanocube samples desorbs neutral Mg atoms with hyperthermal kinetic energies in the range of 0.1–0.4 eV. Our *ab initio* calculations suggest that metal atom emission is induced predominantly by electron trapping at surface three-coordinated Mg sites followed by electronic excitation at these sites. The proposed general mechanism can be used to control atomic-scale modification of insulating surfaces.

DOI: [10.1103/PhysRevB.74.045404](https://doi.org/10.1103/PhysRevB.74.045404)

PACS number(s): 68.47.Jn, 73.22.-f, 71.35.-y, 79.20.La

**I. INTRODUCTION**

Control over surface morphology and chemical reactivity is a major challenge in developing new technologies. It is desirable to modify the geometric and electronic structures and hence the chemical reactivity of metal oxides, on an atomic scale, to create tailored surface structures for technological, analytical, and catalysis applications. Nonselective optical absorption at metal oxides, for example, MgO crystals, induces a wide range of processes including desorption of atoms, ions, and molecular species.<sup>1–3</sup> Controlled surface modification requires better understanding of fundamental mechanisms that convert photon energy into selective bond breaking and desorption from particular surface sites. Such mechanisms have been suggested for semiconductor<sup>4</sup> and metal surfaces.<sup>5</sup> Practical methods for controlling velocity and electronic state distributions of halogen atoms desorbing from alkali halide surfaces, by selective excitation of surface excitons, have been reviewed recently.<sup>1</sup> However, using lasers for controlled modification of *metal oxide* surfaces is much more challenging.

To modify atomic-scale surface structures, one needs to gain balanced control over desorption of both oxygen and metal species. Previously, we demonstrated that hyperthermal emission of neutral O atoms from nanostructured MgO films can be induced using 4.66 eV laser pulses.<sup>1,6</sup> The proposed desorption mechanism involves generation of O<sup>−</sup> species selectively at three-coordinated (3C) surface sites—corners and kinks—followed by secondary excitation and O-atom desorption.<sup>1,6</sup> To date, only thermal desorption of neutral metal atoms from gently irradiated ionic materials is reported.<sup>7–9</sup> Here, we describe a process of site-selective hyperthermal metal atom desorption from a metal oxide surface. The details of the desorption mechanism, which we refer to as the “electron plus exciton” mechanism, have been established through theoretical modeling and experimental verification.

Bulk MgO is transparent to UV light below 7.8 eV and has a high radiation damage threshold. In contrast, rough MgO surfaces and powders are sensitive even to low-fluence radiation with photon energies as low as 3.5 eV.<sup>10</sup> Ultraviolet

(UV) excitation also leads to luminescence<sup>10,11</sup> as well as the selective formation of (O<sup>−</sup>) hole centers at 3C anion sites<sup>12</sup> and hyperthermal O-atom emission.<sup>1,6</sup> We demonstrate that similar photon energies can effectively induce neutral metal-atom emission from 3C Mg sites. We apply low-fluence 4.66 eV nanosecond laser pulses to excite nanostructured MgO samples and report neutral ground state Mg-atom (Mg<sup>0</sup>) emission with hyperthermal kinetic energies—a signature of electronic surface excitation.<sup>1</sup> Thus, MgO surfaces can be site selectively chemically activated, by formation of O<sup>−</sup> species, and structurally modified, by removal of O or Mg atoms, using photon energies well below that of the bulk band gap. Only low-fluence laser pulses are required and surface modification can be achieved without significant excitation or modification of the bulk material. These results may lead to development of gentle and general methods for laser modification of oxide surfaces.

The paper is organized as follows. In the next section, we describe the experimental and theoretical methods used in this work. The experimental results are presented in Sec. III and the results of theoretical modeling in Sec. IV. Discussion and conclusions are presented in Sec. V.

**II. EXPERIMENTAL AND THEORETICAL METHODS****A. Experiment**

Hyperthermal Mg<sup>0</sup> emission can take place from any MgO surface, but is most readily observed on samples with large numbers of 3C sites, such as powders and nanostructured films. In our experiments, we study two types of independently characterized MgO samples with high densities of 3C sites. One sample type, grown by chemical vapor deposition (CVD), consists of cubic nanoparticles with edge lengths ranging between 3 and 10 nm.<sup>13</sup> Figure 1(a) shows an atomically resolved transmission electron microscopy (TEM) image showing MgO rocksalt crystal structure and lattice spacing of 4.2 Å. The nanocubes display shapes deviating from the perfect cube geometry and a large number of corner sites. The physical and optical properties of MgO nanocubes are very well characterized.<sup>10–14</sup>

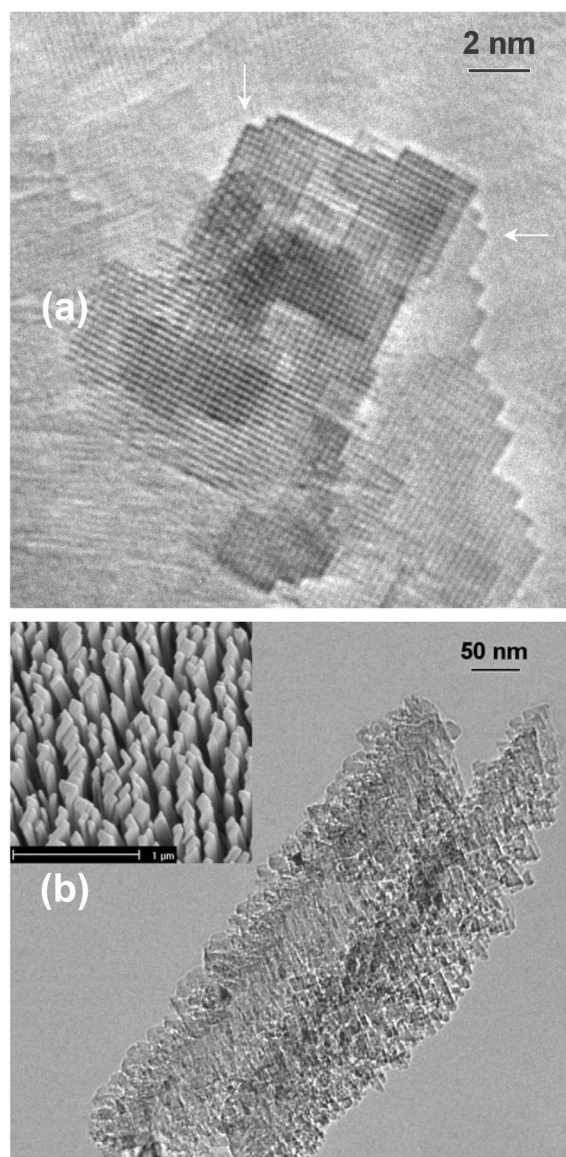


FIG. 1. Electron microscopy of MgO nanocubes grown by the CVD technique and MgO thin films grown by the RBD technique: (a) High-resolution TEM image of MgO nanocubes displaying the crystalline structure and morphology with arrows indicating 3C corner sites. (b) SEM image showing the top view of an MgO film (inset). The Bright-field TEM image of two MgO-columns demonstrates that the film consists of highly porous columns with large numbers of low-coordinated sites at the column surface.

As the second sample, we used  $\sim 600$  nm thick films of MgO grown at room temperature by reactive ballistic deposition (RBD) (Refs. 15 and 16) on cleaved LiF crystals. This growth technique creates very high surface area films. Figure 1(b) shows a scanning electron microscopy (SEM) image, of a typical MgO film, revealing the columnar film structure (inset), while the bright-field TEM image displays many low-coordinated sites on two individual nanocrystalline columns. The stoichiometry and crystallographic orientation of RBD-grown films has been characterized by x-ray photoelectron spectroscopy (XPS) and x-ray diffraction.<sup>15,16</sup>

Laser excitation experiments are carried out under ultra-high vacuum conditions (base pressure  $< 10^{-9}$  Torr) using the output of a frequency quadrupled nanosecond Nd:yttrium aluminum garnet (YAG) pulses to excite MgO surfaces with low-fluence ( $2\text{--}4$  mJ/cm<sup>2</sup>) 4.66 eV photons. Desorbed Mg<sup>0</sup> atoms are ionized by a delayed probe laser focused approximately 0.4 cm above, and oriented parallel to, the sample surface. The probe laser (a frequency doubled Nd:YAG pumped dye laser tuned to the Mg  $3s^2\ ^1S_0 \rightarrow 3s3p\ ^1P_1$  transition at 285 nm) efficiently ionizes Mg<sup>0</sup> atoms using a (1 + 1) resonance-enhanced scheme for subsequent analysis by time-of-flight mass spectrometry.

## B. Theory

To model the Mg-atom desorption mechanism, we employed the same *ab initio* embedded cluster method as used previously.<sup>6</sup> This method is implemented in the computer code GUESS, which is described in detail elsewhere.<sup>17,18</sup> Briefly, we consider a cluster of ions treated quantum mechanically [QM cluster as shown in Fig. 3(b)] embedded in a cubic nanocluster of polarizable classical ions treated using a shell model.<sup>18</sup> An MgO nanocrystalline particle was modeled using a cubic nanocluster of  $10 \times 10 \times 10$  ions. The nanocluster was divided into three regions: a QM cluster, a classically treated region, and an interface between them. All the classical ions interact among themselves via interatomic potentials. The interface atoms interact quantum mechanically with atoms in the QM cluster and classically with other interface atoms as well as with the classical atoms of the nanocluster. In addition, a short-range interaction between the classical atoms and the atoms of the QM cluster is introduced. All centers (i.e., nuclei of quantum ions and cores and shells of classical ions) in the nanocluster are allowed to relax simultaneously during the geometry optimization. The stoichiometric QM cluster Mg<sub>13</sub>O<sub>13</sub> shown in Fig. 3(b) was used in all calculations. An interface layer between the QM cluster and the classically treated ions is needed in order to prevent an artificial spreading of electronic states outside the QM cluster. The interface includes 36 Mg<sup>2+</sup> ions (hereafter denoted as Mg\*); these are represented using a semilocal effective core pseudopotential (ECP).<sup>19</sup>

The GUESS code<sup>17,18</sup> provides the shell model representation for the classically treated part of the system, and an interface with the GAUSSIAN 03 package<sup>20</sup> for *ab initio* calculations of the QM cluster. The calculation of the total energy has been described in detail previously.<sup>18,21</sup> The GUESS code allows one to calculate forces acting on all centers in the nanocluster and simultaneously optimize their positions. The total energy and the electronic structure of the QM cluster are calculated by solving standard Kohn-Sham equations, which include the matrix elements of the electrostatic potential due to all classical point charges in the nanocluster computed on the basis functions of the cluster. We used a modified gradient corrected Becke's three-parameter hybrid exchange functional<sup>22</sup> in combination with the correlation functional of Lee, Yang, and Parr<sup>23</sup> (B3LYP). The parameters of the classical shell model potentials used in this work were optimized to reproduce the properties of small MgO clusters

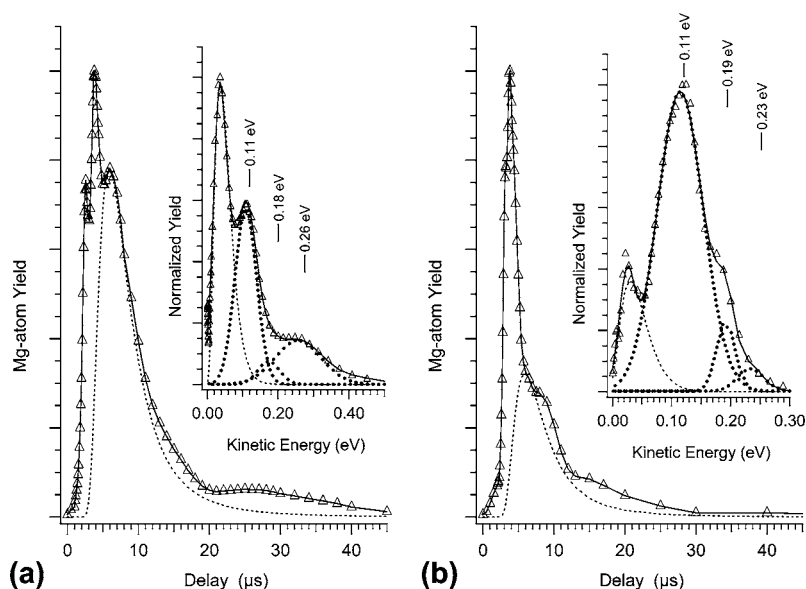


FIG. 2. Velocity profile and kinetic energy distribution of  $\text{Mg}^0$  atoms following irradiation with 4.66 eV photons and a laser fluence of  $4 \text{ mJ/cm}^2$  from: (a) MgO nanocube and (b) RBD thin film samples. The insets show the corresponding  $\text{Mg}^0$  atom kinetic energy distributions obtained by transformation of the velocity profiles; hyperthermal components at  $\sim 0.11$ ,  $\sim 0.18$ , and  $\sim 0.25$  eV are evident. The dotted line in the velocity profiles represents a Maxwell-Boltzmann fit of the thermal emission component ( $T = 300 \text{ K}$ ).

calculated quantum mechanically.<sup>24</sup> The standard 6-31 G basis set for QM cluster Mg and O atoms was used in most calculations. No basis functions were set on the interface  $\text{Mg}^*$  atoms. The surface excitation energies were calculated using time-dependent density functional theory (TD-DFT) as implemented in the GAUSSIAN 03 code.<sup>20</sup>

### III. EXPERIMENTAL RESULTS

Velocity profiles are obtained by measuring the relative  $\text{Mg}^0$  yield as a function of delay between pump and probe lasers as displayed in Fig. 2. XPS spectra do not indicate any metallization of the MgO-film surface under prolonged laser irradiation at laser fluences typically used in our studies. As an experimental test, measurements of Mg-atom desorption are performed on Mg metal films with similar irradiation fluences as on MgO samples. The resulting Mg-atom velocity distribution fits a thermal Maxwell-Boltzmann distribution. This result agrees with other studies reporting thermal desorption from metal targets irradiated by nanosecond laser pulses.<sup>25</sup> Therefore, we attribute all hyperthermal  $\text{Mg}^0$  desorption to excitation of stoichiometric MgO samples.

The RBD-grown thin films and CVD-grown nanocubes readily photodesorb Mg atoms under low-fluence 4.66 eV laser excitation. Figure 2 displays  $\text{Mg}^0$  velocity profiles measured for MgO nanocubes and thin films. The velocity profiles can be transformed into kinetic energy distributions by means of the instrument source function. The deconvolution of the resulting kinetic energy distributions show significant hyperthermal components with distinct peaks centered at  $\sim 0.11$  eV,  $\sim 0.18$  eV, and  $\sim 0.25$  eV. The  $\text{Mg}^0$  velocity distributions also display a significant thermal component whose origin is not yet understood. Here, we focus on the hyperthermal  $\text{Mg}^0$  emission mechanism. Hyperthermal emission must originate from the sample surface (or near surface) as diffusion of Mg atoms from the bulk would lead to thermal emission distributions.

At low laser power, it is possible to desorb Mg atoms without simultaneously desorbing either  $\text{Mg}^+$  or  $\text{Mg}^{2+}$  ions.

For both thin films and nanocubes, the Mg-atom yield displays a nonlinear dependence on the excitation laser fluence,  $P^n$ , of  $n=3$ —indicative of a three-photon process. The Mg-atom detection threshold is  $\sim 1.1 \text{ mJ/cm}^2$  but varies with surface morphology, i.e., it appears to depend on the concentration of low-coordinated surface sites. The Mg-atom desorption threshold is the lowest on RBD-grown MgO films due to their large surface area [ $750\text{--}1000 \text{ m}^2/\text{g}$  (Ref. 15)] and high 3C site density,  $\sigma_{3C}$ , estimated to be in the order of  $\sim 10^{20} \text{ g}^{-1}$ . In contrast, desorption studies on nanocubes require somewhat higher laser fluences than found for the RBD MgO films. Typical cube sizes range between 3 and 10 nm and surface areas are measured to be between  $300\text{--}400 \text{ m}^2/\text{g}$ .<sup>12-14</sup> The value of  $\sigma_{3C}$  is expected to be at least one order of magnitude lower for CVD nanocube samples than that for the RBD-grown films ( $\sigma_{3C} \approx 10^{19} \text{ g}^{-1}$  or  $4 \times 10^{17} \text{ g}^{-1}$  for 3 and 10 nm size cubes, respectively). The suggested dependence of Mg-atom desorption threshold on 3C surface-site density correlates well with optical absorption experiments<sup>26</sup> where the intensity of the absorption band at 4.6 eV, attributed to the excitation of 3C anion sites, was determined to depend on the  $\sigma_{3C}$  value.

### IV. THEORETICAL MODELING RESULTS

Desorption of  $\text{Mg}^+$  and  $\text{Mg}^{2+}$  ions with high kinetic energies has been observed following intense UV irradiation of MgO.<sup>2,3</sup> However, the ion desorption mechanism is distinctly different from the neutral desorption mechanism discussed here. Recently, two mechanisms were suggested for the hyperthermal desorption of neutral oxygen atoms: a double-excitation mechanism and a mechanism that requires sequential hole trapping and excitation at 3C oxygen sites.<sup>1,6</sup>

Since experiments and theory<sup>10-12,17,6</sup> demonstrate that 4.66 eV photons can selectively excite 3C surface sites, and cause desorption of neutral O and Mg atoms, we initially focus on desorption from a simple Mg corner site formed by the intersection of three (001) planes. Our results obtained for this system suggest that two mechanisms could be re-

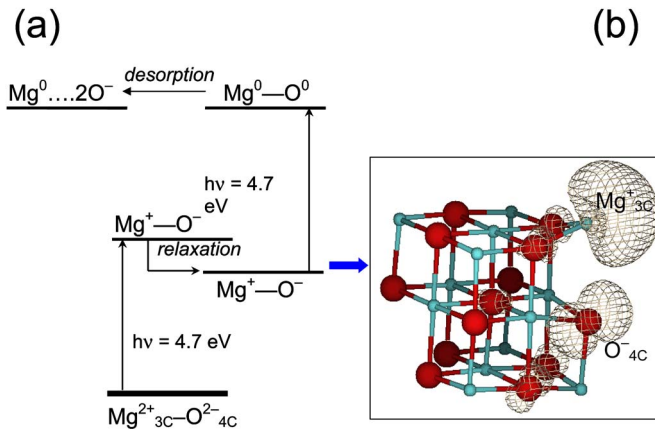


FIG. 3. (Color online) Schematic representation of Mg-atom desorption via biexciton mechanism: (a) the total energy levels of many-electron states involved in the desorption mechanism, and (b) a surface of constant spin-density value calculated for the states of fully relaxed triplet exciton ( $\text{Mg}^+-\text{O}^-$  configuration) shown on the background of the QM cluster. Thick and thin horizontal lines show the ground and excited states of the system respectively. The processes involved are indicated with arrows.

sponsible for the hyperthermal Mg atom desorption. The first mechanism, which we refer to as a “biexciton” mechanism (see Fig. 3), involves two localized electron transfer transitions caused by two sequential optical excitations at an  $\text{Mg}^{2+}$  corner. The lowest intense singlet  $\rightarrow$  singlet transitions have calculated energies of 4.7 eV and 4.8 eV (see also Ref. 6). The corresponding excited state is due to electron transfer from four-coordinated O ions at the cube edges to the 3C  $\text{Mg}^{2+}$  ion at the corner. The system then can relax to the lowest triplet excited state. Both electron and hole components in the lowest triplet excited state are localized at the adjacent Mg corner and one of the edge O ions respectively, so their electrostatic attraction lowers the total energy. The relaxation of this state is accompanied by the 1.2 Å displacement of the corner  $\text{Mg}^+$  ion out of the surface along the (100) axis forming an  $\text{Mg}^+\dots\text{O}^-$  configuration [see Fig. 3(b)].

Without further excitation, this excited state will decay through either radiative or nonradiative transitions to the ground state. However, if the photon fluence is high enough, yet another photon can interact with this excited state prior to its decay. The calculated vertical ionization energy of the lowest triplet excited state at the equilibrium configuration is about 4.6 eV, roughly the laser photon energy. Our calculations show that a second excitation at  $\sim 4.8$  eV should result in the formation of an excited state, which relaxes with spontaneous desorption of  $\text{Mg}^0$  with kinetic energy near 0.3 eV. Thus, the second excitation may result either in ionization of the first excited state or in its excitation into a higher excited state and subsequent desorption [see Fig. 3(a)]. The likelihood of exciton ionization over a second excitation process suggests that the biexciton mechanism may not be very efficient if one uses only 4.66 eV photons, as in the present case.

The alternative “electron plus exciton” mechanism, schematically presented in Fig. 4, involves initial trapping of an “extra” electron at a 3C  $\text{Mg}^{2+}$  site. Electron trapping at MgO surfaces and formation of 3C  $\text{O}^-$  species in MgO nanocrystals,

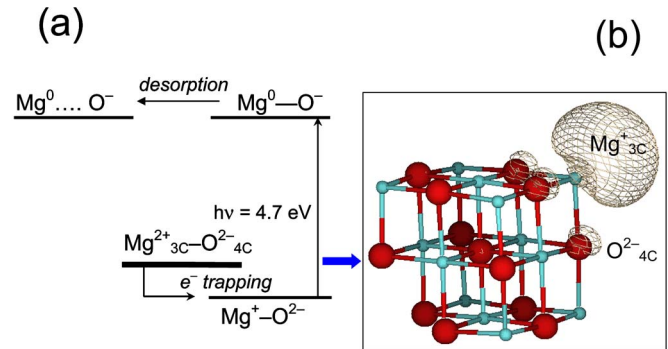


FIG. 4. (Color online) Schematic representation of Mg-atom desorption via electron-plus-exciton mechanism: (a) the total energy levels of many-electron states involved in the desorption mechanism, and (b) a surface of constant spin-density value calculated for the state of an extra electron trapped at the 3C Mg site ( $\text{Mg}^+$  configuration) shown on the background of the QM cluster. Other notations are the same as in Fig. 3.

by 4.7 eV photons, has been verified by EPR studies.<sup>12</sup> Our calculations show<sup>18,21</sup> that 3C  $\text{Mg}^{2+}$  sites have a positive electron affinity and can serve as shallow electron traps. The trapped electron is fully localized on the remote Mg corner site [see the spin density plot in Fig. 4(b)] and its ionization energy is about 1 eV. This state can be either ionized or further photoexcited by an additional 4.7 eV photon, effectively transferring an electron from a neighboring  $\text{O}^{2-}$  ion. The calculations demonstrate that such an excitation creates an  $\text{Mg}^0$  atom, which can be spontaneously desorbed with a kinetic energy near 0.2 eV.

We note that the “extra” electron can originate either from photoionization of a 3C  $\text{O}^{2-}$  site<sup>1,6</sup> or from photoionization of a 3C  $\text{Mg}^+\dots\text{O}^-$  configuration formed as described in the initial step of the biexciton mechanism. In either case, formation of the extra electron requires two 4.66 eV photons.

## V. DISCUSSION AND CONCLUSIONS

Photo- and electron-stimulated desorption of insulators has been studied for long time; this is a rare case where desorption of *metal atoms with hyperthermal velocities* is observed. We show that the hyperthermal Mg atoms originate from a dynamical process rather than thermal evaporation. Desorption of both O and Mg atoms means that (i) contrary to common perception, oxide surfaces *are* modified during even mild irradiation with photons within the bulk transparency range, and (ii) it may be possible to control the surface desorption and engineer new structures on oxides if one knows the photon energies required for desorbing particular surface features.

Both mechanisms described above predict hyperthermal desorption of Mg atoms. However, since the 3C  $\text{Mg}^+$  state is short-lived, different yield versus power dependences are predicted for them. The biexciton mechanism requires only two photons while the “electron plus exciton” mechanism requires three: two photons are required to create an extra electron, and one to excite the  $\text{Mg}^+$  corner. Therefore, the measured yield versus power dependence of  $P^3$  is most con-

sistent with the “electron plus exciton” mechanism. There exist a variety of 3C structural types, such as step corners and kinks, beyond the simple geometry of a perfect Mg corner. We find that this mechanism also predicts the desorption of these other types of 3C sites and that the kinetic energies of desorbing Mg atoms depend on the 3C site structure. Taken together, the electron-plus-exciton mechanism explains the multiple hyperthermal Mg<sup>0</sup> kinetic energy distributions, the variation of Mg<sup>0</sup> yields between different sample type, and the power dependence of Mg<sup>0</sup> desorption. We note that the 3C O<sup>-</sup> species left on the surface after the Mg atom desorption serve as precursors for further O atom desorption.<sup>1,6</sup> This suggests the possibility of correlated sequential Mg and O atom desorption.

To summarize, using selective 4.66 eV laser excitation of RBD-grown MgO thin films and CVD nanocube MgO samples, we have observed hyperthermal Mg desorption. The experimental results are consistent with an electron-plus-exciton desorption mechanism for 3C Mg surface sites. The proposed elementary mechanism involves both sequential excitation and localization of excitons as well as electrons and holes at 3C surface sites. This mechanism differs from all previously suggested mechanisms for desorption induced by electronic transitions.<sup>1,4,5</sup> The desorption process is a remarkable demonstration of local rearrangement of the electronic structure of ionic divalent material in which two electrons are transferred to a single Mg<sup>2+</sup> site to break the

ionic bond and initiate desorption. The Mg- and O-atom desorption process provides an example of atomic-scale modification of a nanostructured metal oxide using laser light tuned to excite specific surface sites at energies well below the excitation threshold of the bulk material. The proposed mechanisms are likely to be general to a wider group of metal oxides as we recently observed UV laser desorption of hyperthermal O atoms induced from RBD-grown CaO films. Thus, the described desorption processes take place at other oxide surfaces and could possibly be used for their modification.

#### ACKNOWLEDGMENTS

The authors were supported by the Department of Energy, Divisions of Chemical Sciences of the Office of Basic Energy Sciences. Pacific Northwest National Laboratory is operated for the U.S. Department of Energy by Battelle. Experiments were performed in the Environmental Molecular Sciences Laboratory, a U.S. Department of Energy user facility operated by the office of Biological and Environmental Research. P.V.S. is supported by the Grant-in-Aid for Creative Scientific Research (Grant No 16GS0205) from the Japanese Ministry of Education, Culture, Sports, Science and Technology. We are grateful to E. Knözinger and O. Diwald for providing us with samples of MgO nanocubes, and to K. Tanimura for valuable discussions.

- <sup>1</sup>W. P. Hess, A. G. Joly, K. M. Beck, M. Henyk, P. V. Sushko, P. E. Trevisanutto, and A. L. Shluger, *J. Phys. Chem. B* **109**, 19563 (2005).
- <sup>2</sup>A. G. Joly, W. P. Hess, K. M. Beck, and J. T. Dickinson, *Appl. Surf. Sci.* **186**, 339 (2002).
- <sup>3</sup>S. Kano, S. C. Langford, and J. T. Dickinson, *J. Appl. Phys.* **89**, 2950 (2001).
- <sup>4</sup>J. Kanasaki, T. Ishida, K. Ishikawa, and K. Tanimura, *Phys. Rev. Lett.* **80**, 4080 (1998).
- <sup>5</sup>T. E. Madey and J. T. Yates, Jr., *J. Vac. Sci. Technol.* **8**, 525 (1971); J. T. Yates, Jr., J. Ahner, and D. Mocuta, *Proc. Natl. Acad. Sci. U.S.A.* **95**, 443 (1998).
- <sup>6</sup>P. E. Trevisanutto, P. V. Sushko, A. L. Shluger, K. M. Beck, M. Henyk, A. G. Joly, and W. P. Hess, *Surf. Sci.* **593**, 210 (2005).
- <sup>7</sup>Z. Postawa, R. Maboudian, M. El-Maazawi, M. H. Ervin, M. C. Wood, and N. Winograd, *J. Chem. Phys.* **96**, 3298 (1992).
- <sup>8</sup>J. Kolodziej, P. Czuba, P. Piatkowski, Z. Postawa, V. Kempter, and M. Szymonski, *Vacuum* **45**, 353 (1994).
- <sup>9</sup>K. M. Beck, A. G. Joly, and W. P. Hess, *Phys. Rev. B* **63**, 125423 (2001).
- <sup>10</sup>A. Zecchina, M. G. Lofthouse, and F. S. Stone, *J. Chem. Soc., Faraday Trans. 1* **71**, 1476 (1975).
- <sup>11</sup>S. Coluccia, A. M. Deane, A. J. Tench, *J. Chem. Soc., Faraday Trans. 1* **74**, 2913 (1978).
- <sup>12</sup>O. Diwald, M. Sterrer, E. Knözinger, P. V. Sushko, and A. L. Shluger, *J. Chem. Phys.* **116**, 1707 (2002); M. Sterrer, O. Diwald, E. Knözinger, P. V. Sushko, and A. L. Shluger, *J. Phys. Chem. B* **106**, 12478 (2002).
- <sup>13</sup>E. Knözinger, K. H. Jacob, S. Singh, and P. Hofmann, *Surf. Sci.* **290**, 388 (1993).
- <sup>14</sup>M. Sterrer, Th. Berger, O. Diwald, E. Knözinger, P. V. Sushko, and A. L. Shluger, *J. Chem. Phys.* **123**, 064714 (2005).
- <sup>15</sup>Z. Dohnálek, G. A. Kimmel, D. E. McCready, J. S. Young, A. Dohnáková, R. S. Smith, and B. D. Kay, *J. Phys. Chem. B* **106**, 3526 (2002).
- <sup>16</sup>M. Henyk, K. M. Beck, M. H. Engelhard, A. G. Joly, W. P. Hess, and J. T. Dickinson, *Surf. Sci.* **593**, 242 (2005).
- <sup>17</sup>A. L. Shluger, P. V. Sushko, and L. N. Kantorovich, *Phys. Rev. B* **59**, 2417 (1999).
- <sup>18</sup>P. V. Sushko, A. L. Shluger, and C. R. A. Catlow, *Surf. Sci.* **450**, 153 (2000).
- <sup>19</sup>W. R. Wadt and P. J. Hay, *J. Chem. Phys.* **82**, 284 (1985).
- <sup>20</sup>M. Klene, M. A. Robb, L. Blancafort, and M. J. Frisch, *Chem. Phys.* **119**, 713 (2003); M. J. Frisch, GAUSSIAN 03, Revision B.04, Gaussian, Inc., Pittsburgh, PA, 2003.
- <sup>21</sup>P. V. Sushko, J. L. Gavartin, and A. L. Shluger, *J. Phys. Chem. B* **106**, 2269 (2002).
- <sup>22</sup>A. D. Becke, *J. Chem. Phys.* **98**, 5648 (1993).
- <sup>23</sup>C. T. Lee, W. T. Yang, and R. G. Parr, *Phys. Rev. B* **37**, 785 (1988).
- <sup>24</sup>A. L. Shluger, A. L. Rohl, D. H. Gay, and R. T. Williams, *J. Phys.: Condens. Matter* **6**, 1825 (1994).
- <sup>25</sup>J. Viereck, F. Stietz, M. Stuke, T. Wenzel, and F. Träger, *Surf. Sci.* **383**, L749 (1997).
- <sup>26</sup>S. Stankic, M. Müller, O. Diwald, M. Sterrer, E. Knözinger, and J. Bernardi, *Angew. Chem., Int. Ed.* **44**, 4917 (2005).